Influence of the Indian Ocean Dipole on Atmospheric Subseasonal Variability

TOSHIAKI SHINODA

NOAA–CIRES Climate Diagnostics Center, Boulder, Colorado

WEIQING HAN

Program in Atmospheric and Oceanic Sciences, University of Colorado, Boulder, Colorado

(Manuscript received 9 September 2004, in final form 17 March 2005)

ABSTRACT

The relationship between atmospheric subseasonal variability and interannual variation of SST over the tropical Indian Ocean is examined using winds and humidity from the NCEP–NCAR reanalysis, outgoing longwave radiation (OLR), and the monthly SST analysis. The primary focus is on whether and how the subseasonal variability is related to the zonal dipole structure of SST, which peaks during boreal fall. The level of subseasonal wind activity is measured by standard deviation of bandpass-filtered zonal wind fields on the 6–30- and 30–90-day time scales.

During boreal fall (September–November), the interannual variation of 6–30-day (submonthly) near-surface zonal wind activity in the central and eastern equatorial Indian Ocean is highly correlated with the large-scale zonal SST gradient. The intensity of submonthly variability is largely reduced during positive dipole years. A significant reduction of intraseasonal (30–90-day) wind activity is also evident during large dipole events. However, the correlation with the zonal SST gradient is much weaker than that of submonthly variability.

The mechanism by which the Indian Ocean dipole influences equatorial submonthly winds is investigated based on a cross-correlation analysis of OLR and winds. During negative dipole years, submonthly convection is active in the southeast Indian Ocean where the anomalous convergence of surface moisture associated with dipole events is at its maximum. The submonthly convection in this region is often associated with a cyclonic circulation, and these disturbances propagate westward. Consequently, equatorial westerlies and northwesterly winds near the coast of Sumatra are generated. During positive dipole years, submonthly convective activity is highly reduced in the southeast Indian Ocean, and thus no equatorial westerly is generated.

Ocean response to submonthly disturbances is examined using OGCM experiments forced with winds from the NCEP–NCAR reanalysis. Results suggest that submonthly winds can generate significant upper-ocean response, including strong eastward surface currents near the equator and sea surface height anomalies along the coast of Sumatra where the large SST anomalies associated with dipole events are observed.

1. Introduction

Atmospheric subseasonal variability in the Tropics has been intensively studied in the past few decades because of its importance for tropical climate. While many of the studies focused on the Madden–Julian oscillation (MJO; Madden and Julian 1972), which is responsible for a large portion of subseasonal variability on the time scale of 30–90 days, significant variability on the submonthly time scale (<30 days) has also been reported (e.g., Murakami 1972, 1980; Hartmann et al. 1992; Kiladis et al. 1994; Straub and Kiladis 2003). For instance, Murakami (1980) showed significant spectral peaks in a period range of 15–30 days in outgoing longwave radiation (OLR) over the Indonesian regions. These submonthly fluctuations exhibit eastward propagation and are associated with active winter monsoonal surges. Hartmann et al. (1992) also found a pronounced spectral peak between 20 and 25 days in surface pressure over the western Pacific warm pool during boreal winter, which is shown to be related to the occurrence of typhoons in this region. Recent studies (Kiladis and Wheeler 1995; Wheeler and Kiladis 1999; Wheeler et al. 2000) have demonstrated that a portion of these submonthly convective disturbances can be described in

Corresponding author address: Toshiaki Shinoda, NOAA–CIRES Climate Diagnostics Center, 325 Broadway, Boulder, CO 80305.
E-mail: toshiaki.shinoda@noaa.gov

terms of equatorially trapped wave modes derived by Matsuno (1966). For example, Kiladis and Wheeler (1995) identified the equatorial Rossby modes, which have nearly barotropic structure up to 100 hPa, in 6–30-day-filtered winds for the period 1985–93. Similarly, Numaguti (1995) found submonthly (15–20-day) disturbances during Tropical Ocean Global Atmosphere Coupled Ocean–Atmosphere Response Experiment (TOGA COARE) Intensive Observation Period (IOP; Webster and Lukas 1992), in which the structure and westward phase speed are consistent with equatorial Rossby waves.

Since tropical convection and circulation anomalies over a broad frequency range are strongly tied to large-scale changes in SST (e.g., ENSO), the intensity of subseasonal variability could be modulated by interannual SST fluctuations (e.g., Lau and Chan 1988; Fink and Speth 1997; Hendon et al. 1999). Recent studies have indicated that SSTs in the western Pacific warm pool could influence the location and intensity of atmospheric subseasonal variability (e.g., Bergman et al. 2001; Yu et al. 2003). For instance, Bergman et al. (2001) showed a statistically significant relationship between western Pacific SST anomalies in the boreal fall season and the intensity of intraseasonal (30–90-day) variability in the following winter season. Yu et al. (2003) demonstrated that the activity of westerly wind bursts in the western equatorial Pacific is regulated by zonal SST gradients in the warm pool associated with ENSO through changes of sea level pressure gradient. The intensity of atmospheric subseasonal variability in the tropical Indian Ocean could also be affected by the underlying SST because of its strong interannual variations. However, very little information has been provided about the impact of interannual SST variation in the Indian Ocean on subseasonal variability, particularly for the submonthly time scale.

The interannual variation of SST and winds in the tropical Indian Ocean strongly depends on the season. The anomaly pattern of SST during boreal fall exhibits a zonal dipolelike structure, which is associated with the equatorial zonal wind anomaly (e.g., Saji et al. 1999; Webster et al. 1999). Saji et al. (1999) referred to this zonally out-of-phase SST anomaly pattern as the "Indian Ocean dipole (IOD) mode." While much of the SST anomalies associated with the IOD could be produced remotely by ENSO in the tropical Pacific (Baquero-Bernal et al. 2002; Shinoda et al. 2004a,b), some pronounced IOD events have developed in the absence of well-defined ENSO, supporting the notion that it can arise from air–sea coupled processes inherent in the Indian Ocean (Saji et al. 1999; Webster et al. 1999).

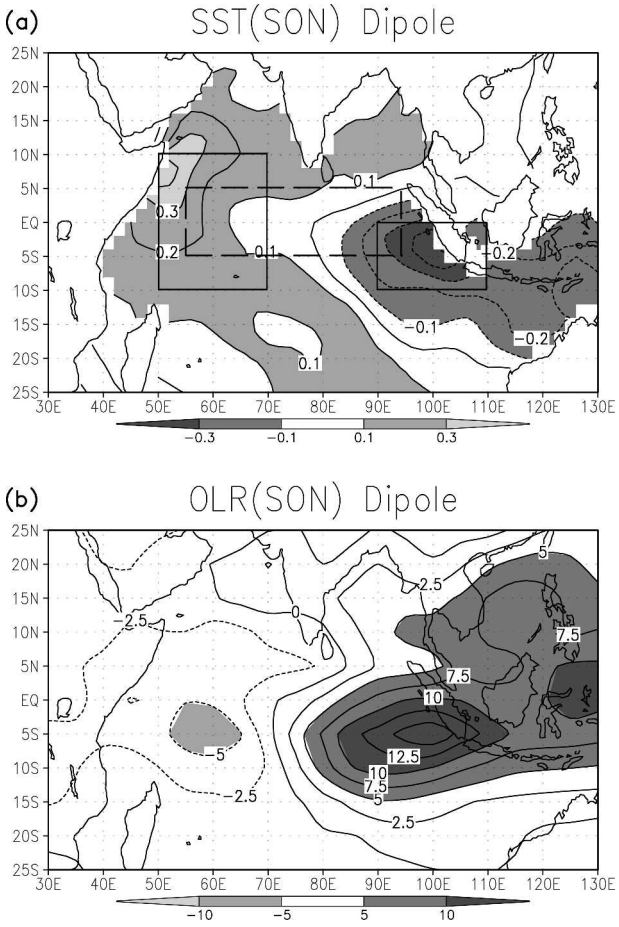

FIG. 1. (a) SSTs during SON regressed onto the DMI defined as the difference in the average SST anomaly between in the western (10°N–10°S, 50°–70°E) and the eastern boxes (0°–10°S, 90°–110°E) shown in the figure. A positive DMI indicates a warmer SST anomaly in the western box. (b) Same as in (a), except for OLR.

Figure 1a shows the average SST during boreal fall [September–October–November (SON)] regressed against the dipole mode index (DMI) defined by the difference of SST anomalies between in the western and eastern boxes shown in the figure (Saji et al. 1999). The meridionally asymmetric pattern of SST anomaly is found in the eastern Indian Ocean where large anomalies are located only in the Southern Hemisphere around 0°–10°S, 100°E, which extends to ~15°S. SST anomalies in the west are weaker and cover most of the western portion of the basin. It is unclear how these large-scale anomalous SSTs and winds associated with IOD events influence, or in turn are influenced by, atmospheric subseasonal variability. The IOD is also associated with anomalous convective activity in the tropical Indian Ocean. Figure 1b shows the average OLR during the SON season regressed against the DMI. Convection in the southeast Indian Ocean is

highly suppressed during positive dipole years (DMI > 0) when cold SST anomalies are found in the east.

Ocean response to atmospheric subseasonal surface forcings in the tropical Indian and Pacific Oceans has been investigated recently through various modeling and data analyses (e.g., Shinoda et al. 1998; Schiller and Godfrey 2003). Subseasonal variations of wind and convection produce significant SST anomalies and upper-ocean currents (e.g., Shinoda and Hendon 1998, 2001; Han et al. 2001; Han 2005), and they can further affect longer time-scale phenomena such as ENSO and IOD (e.g., Kessler and Kleeman 2000; Shinoda and Hendon 2002; Waliser et al. 2003; Han et al. 2004). For instance, Han et al. (2004) demonstrated that subseasonal winds in the Indian Ocean can generate a lower-frequency component of equatorial jet (Wyrtki 1973) because of nonlinear processes in the upper ocean. Hence, the subseasonal winds (especially near the equator) could play an important role in regulating longer time-scale variations in the tropical Indian Ocean including interannual variability such as the IOD.

Based on previous studies described above, oceanic and atmospheric subseasonal and interannual variability in the tropical Indian Ocean could significantly influence each other, and therefore simulating interannual variations may require accurate forecast of the activity of atmospheric subseasonal variability. Accordingly, knowledge of the relation between subseasonal and interannual variability and the mechanism responsible for the interaction may be crucial for predicting interannual variations in the tropical Indian Ocean. In this study, we will first investigate whether and how interannual SST variations over the tropical Indian Ocean are related to atmospheric subseasonal variability using the National Centers for Environmental Prediction–National Center for Atmospheric Research (NCEP–NCAR) reanalysis (Kalnay et al. 1996) winds and humidity, OLR, and monthly SST analysis. We will focus on subseasonal variability during the boreal fall season when the SST dipole structure dominates the interannual variation. Since we found that the IOD is strongly correlated with submonthly (6–30 day) variability, further analyses were conducted to examine the mechanism by which the IOD influences winds and convection on this time scale. The impact of subseasonal winds on upper-ocean variability will also be discussed based on ocean general circulation model (OGCM) experiments forced with observed winds.

2. Data

Three primary datasets are used in this study. Daily average OLR from the Advanced Very High Resolution Radiometer (AVHRR) on the National Oceanic and Atmospheric Administration's (NOAA's) operational polar orbital satellite (Gruber and Krueger 1984) is used as a proxy for deep convection. The data for the 22-yr period of 1979–2001 with horizontal resolution of 2.5° are analyzed. Daily winds, humidity, and geopotential height at 1000 hPa from the NCEP–NCAR reanalysis (Kalnay et al. 1996) for the period 1948–2001 are analyzed to provide information on circulations associated with tropical subseasonal variability and the interannual variation of near-surface humidity. The datasets are global, with 2.5° spatial resolution. The NCEP–NCAR reanalysis winds on the subseasonal time scale were previously evaluated by comparing them with direct measurements, National Aeronautics and Space Administration (NASA) Scatterometer (NSCAT) data and other independent estimates, showing that they capture subseasonal variability over the tropical Indian and western Pacific Oceans reasonably well (Shinoda et al. 1999; Han et al. 2004). The monthly SSTs from the analysis of Smith and Reynolds (2004) are used to describe interannual SST variations. The data for the period 1950–2001 with 2° horizontal resolution are analyzed.

Wind and geopotential height anomalies are filtered into three bands: 6–90, 30–90, and 6–30 days using a Lanczos digital filter (see Duchon 1979). The annual cycle was removed from daily averaged data prior to filtering. Winds and convection in the tropical Indian Ocean reveal high variability on all time scales from interannual to less than daily. The 6–90-day band represents most of the subseasonal variability. Six days was chosen as the high end of frequency for the filter to remove signals of westward-propagating disturbances with the period around 2–5 days (e.g., Reed and Recker 1971; Liebmann and Hendon 1990; Takayabu and Nitta 1993; Dickinson and Molinari 2002). The 30–90-day band is dominated by fluctuations associated with the MJO. The variability of a higher frequency (6–30 days) band consists of a variety of phenomena including westerly wind bursts, tropical cyclones, tropical wave activity, and a quasi-biweekly oscillation (e.g., Murakami and Frydrych 1974; Lyons 1981; Kiladis et al. 1994; Wheeler and Kiladis 1999; Chatterjee and Goswami 2004). Filtered and unfiltered time series of all variables are analyzed just for the SON season when SST dipole variability is at its maximum.

3. Interannual variation of subseasonal variability

To measure the intensity of subseasonal variability, standard deviations of the bandpass-filtered time series during the SON season are calculated for each year.

The level of variability (as measured by its standard deviation) of zonal wind averaged over the equatorial area (5°N–5°S, 55°–95°E) is compared with the DMI and the local SST (Table 1; Fig. 2). The correlation coefficients (rr) of subseasonal activity with the DMI and the average SST in the same area for each subseasonal band are listed in Table 1. The activity of the subseasonal zonal wind on the time scale of 6–90 days is highly correlated with the DMI (rr = 0.75; Fig. 2a). Significant reduction of subseasonal wind activity is found during the positive (cooling in the east) IOD years including ENSO-independent dipole events (e.g., 1961). The correlation of the DMI with 6–30-day wind activity is similar to that with 6–90-day wind activity (rr = 0.68; Fig. 2b). While the correlation of 30–90-day (the time scale of the MJO) zonal wind activity with the DMI is statistically significant (95%; rr = 0.45), the correlation is much weaker than that with the activity of 6–30-day variability (Fig. 2c). This suggests that the higher-frequency variability on the time scale of 6–30 days is mostly responsible for the strong correlation of the entire subseasonal (6–90 days) variability with the DMI. The correlation with the local SST is much weaker for all three subseasonal bands (Table 1), suggesting that subseasonal wind activity near the equator is primarily controlled by a large-scale SST gradient.

One interpretation for the stronger correlation of 6–30-day wind activity with the DMI (than with 30–90-day wind activity) is that SST anomalies associated with IOD events may not be broad enough to affect the MJO significantly. The spatial scale of the MJO is global, which is generally larger than higher-frequency variability, and the large SST anomalies during IOD events are observed mostly in the southeastern portion of the basin. Another possible explanation is that the large SST anomalies associated with the IOD, which lasts only 3–5 months, may not be long enough to influence the MJO that has a similar period (~50 days). Also, since the generation mechanism of the MJO and 6–30-day disturbances are apparently different, it is possible that MJO activity is less sensitive to the underlying SST. Nevertheless, some indication of the influence of the SST dipole on the MJO time-scale wind activity is evident. For instance, significant reduction of wind activity on this time scale is found during some large positive IOD years (e.g., 1961, 1982, and 1997).

Previous studies have indicated that SST anomalies in the Indian Ocean associated with the IOD are well correlated with ENSO variability (e.g., Baquero-Bernal et al. 2002). Thus, it is possible that the large-scale circulation anomaly driven by ENSO variability could partly be responsible for the strong correlation between subseasonal wind activity and the DMI. We have also calculated the correlation of subseasonal wind activity with the Niño-3.4 (5°N–5°S, 170°–120°W) SST (Table 1) to examine the ENSO influence on subseasonal winds. The correlations of subseasonal wind activity (for all three subseasonal bands) with the Niño-3.4 SST are much weaker than those with the DMI, suggesting that subseasonal variability is primarily controlled by Indian Ocean SST variability. This is also supported by the fact that a large reduction of subseasonal activity occurred in 1961, which is associated with the strong positive IOD event but not with ENSO. However, it is difficult to isolate the effect of remote forcing by ENSO based only on data analyses because of the strong correlation between the DMI and the Niño-3.4 SST (rr = 0.66).

TABLE 1. Correlation coefficients between subseasonal zonal wind (U) activity, SST in the area (5°N–5°S, 55°–95°E), DMI, and Niño-3.4 SST (see text for details). The data for the period 1950–2001 are used. Linear trends are removed from the time series before the calculations.

Variables	Correlation coefficient
U-wind (6–90 days) vs −DMI	0.75
U-wind (6–30 days) vs −DMI	0.68
U-wind (30–90 days) vs −DMI	0.45
U-wind (6–90 days) vs SST(local)	−0.20
U-wind (6–30 days) vs SST(local)	−0.07
U-wind (30–90 days) vs SST(local)	−0.22
U-wind (6–90 days) vs Niño-3.4	0.53
U-wind (6–30 days) vs Niño-3.4	0.50
U-wind (30–90 days) vs Niño-3.4	0.32
DMI vs Niño-3.4	0.66

The rest of the paper focuses on submonthly (6–30-day) variability because of its stronger correlation with the DMI. The spatial distribution of the correlation between atmospheric submonthly activity and the DMI is examined by calculating the correlation for 5° × 5° grid boxes. Figure 3 shows the correlation of the DMI with activity of submonthly zonal winds and OLR. The maximum (negative) correlation for OLR is located in the southeastern part of the basin around (2.5°–12.5°S, 87.5°–102.5°E). On the other hand, the correlation for zonal winds is at its maximum near the equator and the negative correlation extends farther to the central Indian Ocean near 60°E. This spatial pattern of correlation is important for the ocean response since zonal winds near the equator could produce stronger surface currents (see section 5).

The submonthly convective activity in the southeastern box (2.5°–12.5°S, 87.5°–102.5°E), where the maximum correlation is found, is compared with the DMI (Fig. 4). The large reduction of submonthly convection in this region during positive dipole years is evident

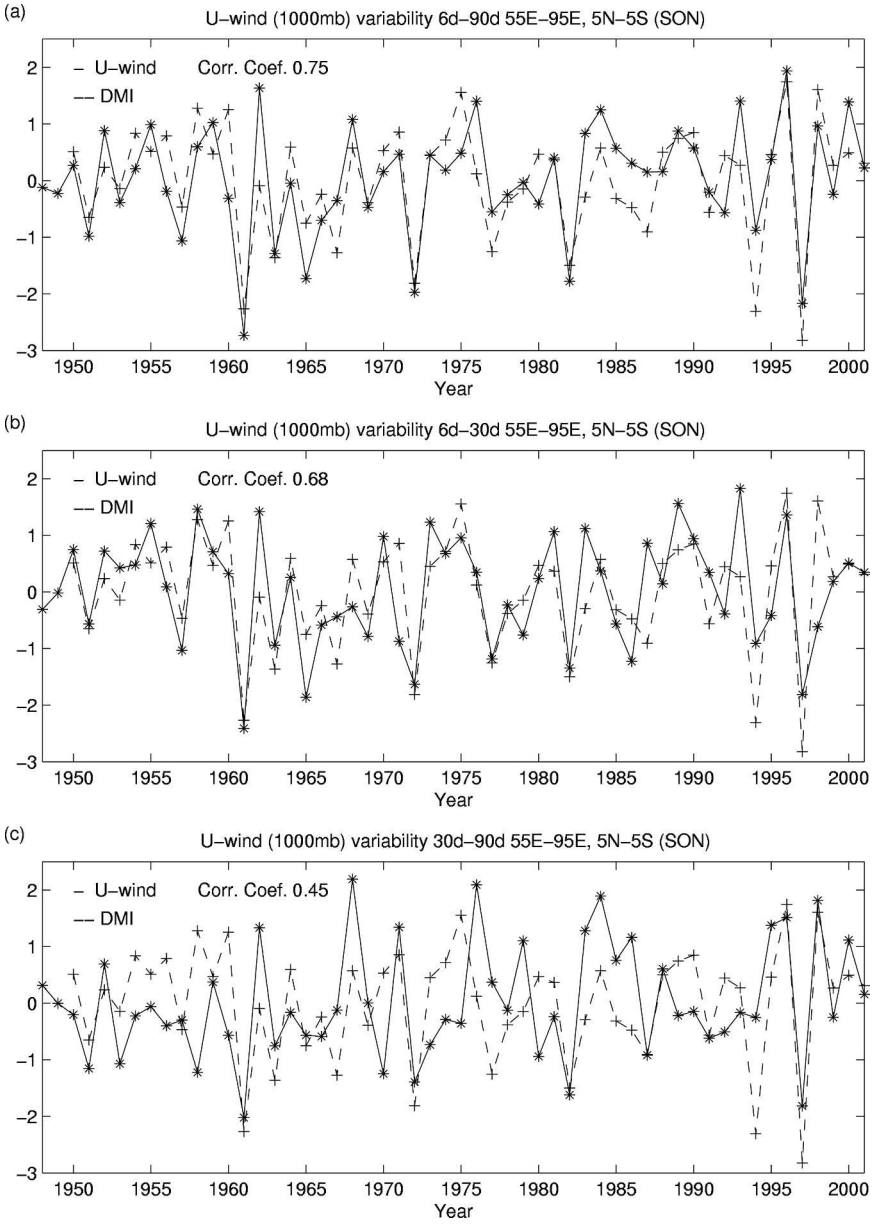

FIG. 2. (a) Variations of the intensity of subseasonal zonal wind variability for the area 5°N–5°S, 55°–95°E (solid line) and the DMI during SON (dashed line). The intensity of the subseasonal zonal wind is measured by the standard deviation of the bandpass-filtered (6–90-day) zonal wind at 1000 hPa. Time series are normalized by their standard deviations, and the means are subtracted. The sign of the DMI is changed for the comparison. (b), (c) Same as in (a), except that zonal winds are bandpass filtered for periods of (b) 6–30 and (c) 30–90 days.

(e.g., 1982, 1994, and 1997). To examine whether this pronounced interannual variation of submonthly convective activity is tied to mean convection in this region, the mean OLR during the SON season is compared with the subseasonal OLR. Figure 5 shows the map of mean OLR and standard deviation of submonthly OLR for the period 1979–2001 and during the large positive IOD years (1982, 1994, and 1997). Active submonthly convection is generally found in the area where the mean convection is active. However, there are some significant differences between mean and submonthly OLR. For instance, the maximum submonthly activity is found around 15°N, 85°E, while the most active mean convection is located around 2.5°N, 100°E. A possible explanation of this difference is that the influence of large-scale SST on convective activity may depend on

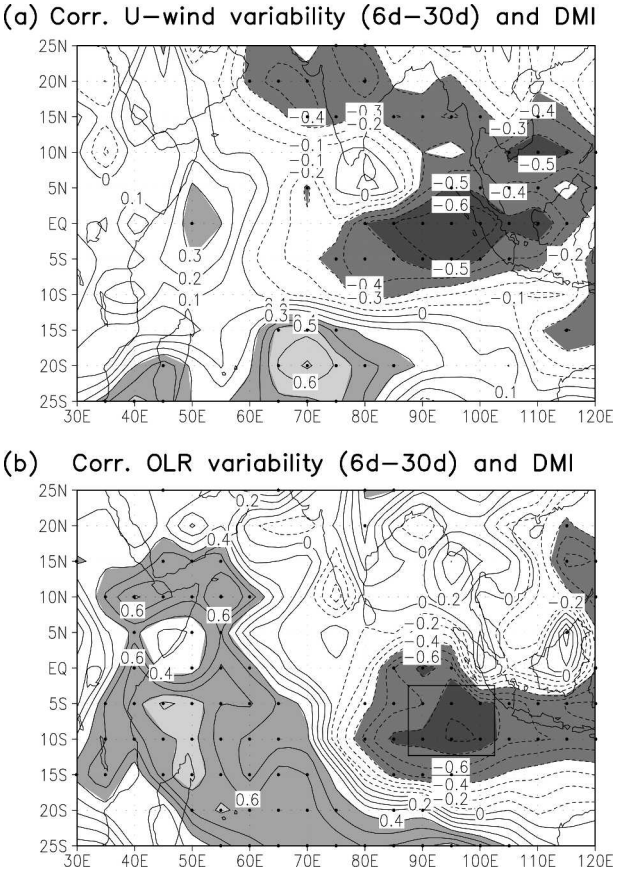

FIG. 3. (a) Correlation coefficient of standard deviation of zonal winds in the 6–30-day band during SON with the DMI. The data for the period 1979–2001 are used for the calculation. Dots indicate the grid points where the correlation is significant at 90% level. (b) Same as in (a), except for the correlation with the standard deviation of 6–30-day OLR.

the time scale. For instance, convection associated the MJO may be affected by underlying SSTs differently compared to submonthly convection.

Both mean and subseasonal convective activity in the southeast Indian Ocean are largely reduced during large positive IOD years (Figs. 5b,d), suggesting that basin-scale SST anomalies associated with IOD events reduced overall convective activity in this region. However, in addition to a large-scale SST gradient, the interannual variation of local SST could also affect convective activity. To examine the relative importance of a large-scale SST gradient and local SST for the convective activity, correlations between mean OLR, submonthly OLR activity, DMI, and SST in the southeast Indian Ocean (average SST in the eastern box shown in Fig. 3) are calculated (Table 2). While these quantities are significantly correlated with each other, there are some notable differences. Both mean OLR and submonthly OLR are best correlated with DMI, and their correlations with the local SST are much weaker. This suggests that large-scale zonal SST gradients and wind anomalies associated with IOD events are more important for controlling overall activity of convection in this region.

A possible explanation of these relationships is that SST gradient and surface wind anomalies associated with IOD affect submonthly convective activity through the interannual variation of surface moisture convergence in this region. During negative IOD years, the convergence of surface moisture caused by large-scale wind anomalies may enhance both mean and subseasonal convective activity in the southeast Indian Ocean. To examine this mechanism, the surface moisture divergence defined by $\nabla \cdot (q\mathbf{U})$ (where q is the specific humidity and $\mathbf{U}$ is the wind vector at 1000 hPa) is compared with IOD variability. Figures 6a and 6b show the average surface wind and moisture divergences during the SON season regressed onto the DMI The spatial patterns of these figures (Figs. 6a,b) are nearly identical, suggesting that large-scale moisture convergence is primarily controlled by surface wind variability. The maximum moisture divergence anomaly is found in the southeast Indian Ocean around 10°S, 90°–100°E, indicating that the moisture convergence in this region is highly reduced during large positive IOD years because of large-scale wind anomalies associated with the IOD (Fig. 6c). The meridional component of wind anomaly is largely responsible for the anomalous moisture divergence in this region. The location of maximum moisture divergence anomaly coincides with the area where the correlation between submonthly convective activity and the DMI is at its maximum (Fig. 3b). This suggests that the reduced convergence of surface moisture during large positive IOD events is responsible for the suppressed submonthly convection in this region.

Table 2 also shows correlations of $\nabla \cdot (q\mathbf{U})$ with mean OLR, submonthly OLR activity, DMI, and the local SST in the southeast Indian Ocean. Note that all values in Table 2 are calculated from the data for the period 1979–2001, while Fig. 6c shows the time series for the period 1950–2001. The surface moisture divergence in this region is better correlated with the large-scale SST gradient (DMI) than with the local SST, which is similar to the relationship between submonthly OLR variability, DMI, and the local SST. In addition, the moisture divergence is highly correlated with submonthly convective activity (rr = 0.82).

While these analyses indicate that large-scale surface wind anomalies associated with SST gradients primarily control the surface moisture convergence in the southeast Indian Ocean, convective activity in this region

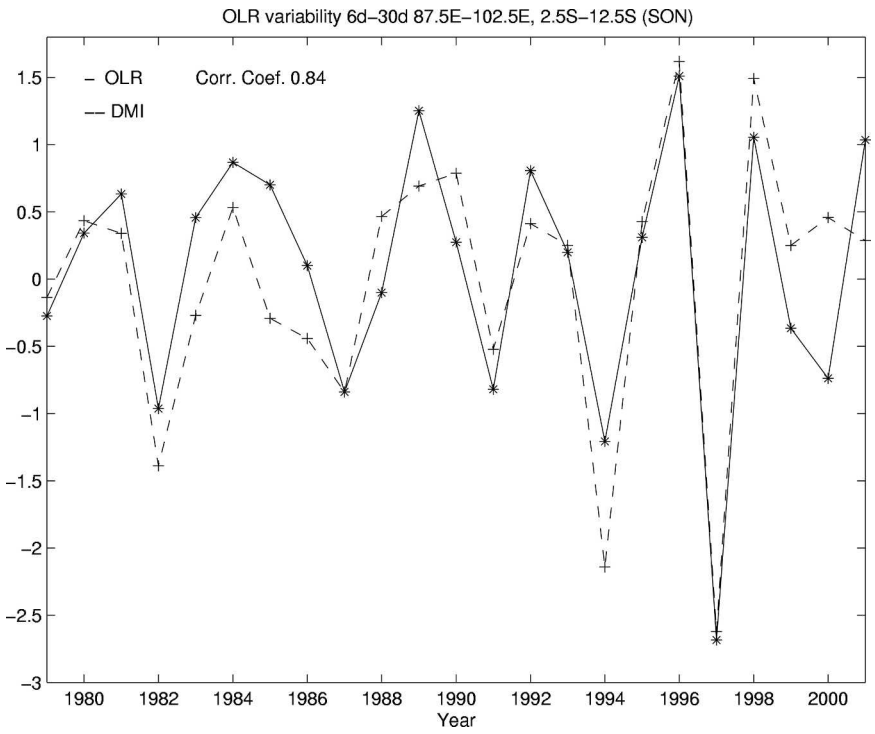

FIG. 4. Variation of the intensity of the submonthly (6–30 days) OLR variability for the area 2.5°–12.5°S, 87.5°–102.5°E (solid line), and of the DMI (dashed line) during SON. The intensity of OLR variability is measured by standard deviation of the bandpass-filtered (6–30-day) time series. Time series of the SON mean are normalized by their standard deviations, and the means are subtracted. The sign of DMI is changed for the comparison.

could also be influenced by surface evaporation through changes of local SST. However, during positive IOD years, evaporative cooling is generally increased due to the enhanced wind speed in the southeast Indian Ocean because anomalous southeasterlies in this region act to increase the climatological winds during boreal fall (e.g., Shinoda et al. 2004a). Hence, it is unlikely that the interannual variation of convective activity in this region is largely controlled by surface evaporation. However, this does not imply that the local SST has no impact on convective activity. Since DMI is strongly correlated with the local SST (rr = 0.9) and these two variables are not independent, it may not be possible to isolate and quantify variability of submonthly convective activity caused solely by the local SST variation by statistical analyses. Atmospheric model experiments that prescribe different SSTs are necessary to further examine this problem.

4. Evolution of subseasonal winds

In the previous section, it was demonstrated that submonthly convective activity in the southeast Indian Ocean is strongly influenced by basin-scale SST gradients and surface wind anomalies associated with IOD events. In this section, circulation anomalies associated with the submonthly convective activity in this region are described based on the cross-correlation analysis. In addition, an example that illustrates many features of submonthly variability identified by the statistical analysis is provided.

a. Cross-correlation analysis

Time series of 1000-hPa winds and geopotential height are regressed onto the filtered OLR (6–30 days) averaged over the box shown in Fig. 3b to describe the pattern and evolution of wind variability associated with the submonthly convection in the southeast Indian Ocean. Similar techniques were used in many studies on subseasonal variability of convection and circulation (e.g., Kiladis and Weickmann 1992; Hendon and Liebmann 1994; Mathews and Kiladis 1999). Fourteen years of filtered (6–30 days) time series during negative dipole years (DMI < 0) are first used to create the "composite" circulation anomaly associated with submonthly convective activity in the southeast Indian Ocean, which are not affected by large positive IOD events. The statistical significance of cross correlation is calculated

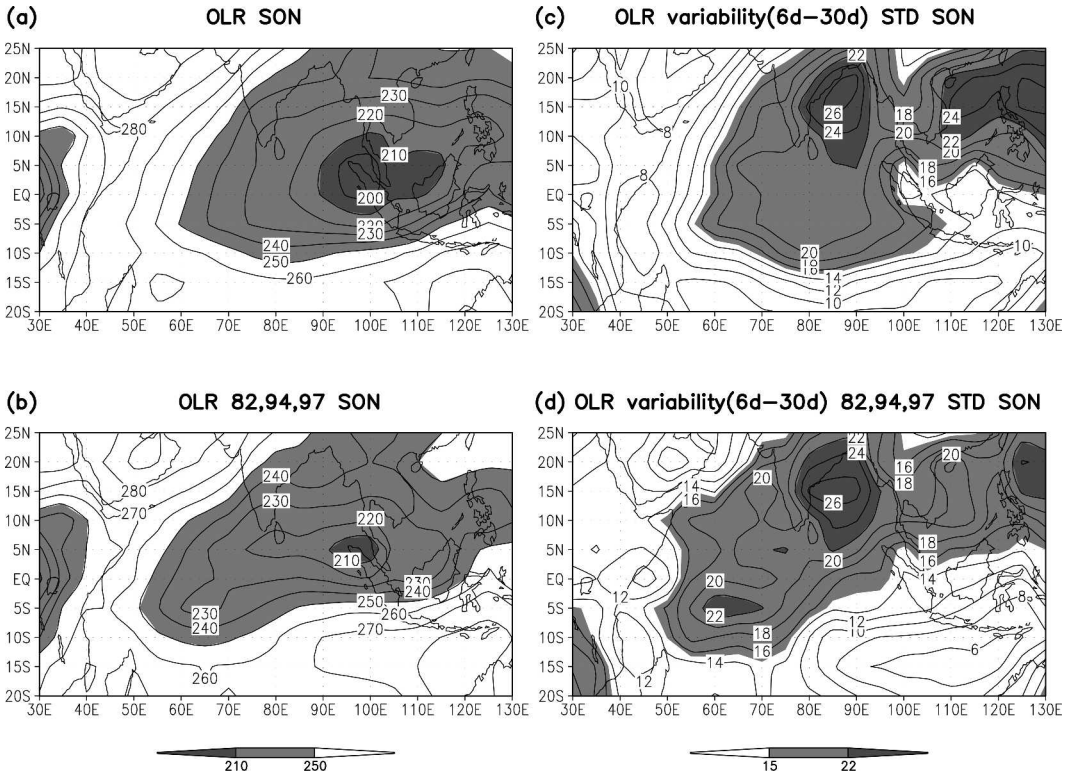

FIG. 5. (a) Mean OLR (W m^{-2}) during SON for the period 1979–2001. (b) Same as in (a), except for the period 1982, 1994, and 1997. (c) Standard deviation of submonthly (6–30 days) OLR during SON for the period 1979–2001. (d) Same as in (c), except for the period 1982, 1994, and 1997.

with a reduced number of the degrees of freedom based on temporal autocorrelation characteristics of filtered time series (Oort and Yienger 1996).

Figure 7 shows the relationship between 6–30-day OLR in the base region (2.5°–12.5°S, 87.5°–102.5°E) and the 1000-hPa circulation, and the geopotential height anomalies in the tropical Indian Ocean. "Day 0" in Fig. 7 represents the contemporaneous relationship that describes the circulation and the height anomalies when the strong deep convection occurs in the base region. On day −2, a cyclonic circulation associated with negative height anomalies begins to develop in the southeast Indian Ocean around 5°S, 95°E. This cyclonic circulation is associated with a weaker anticyclonic circulation and positive height anomalies around 15°S, 80°E. Strong southeasterlies are generated between the cyclonic and anticyclonic circulations. As these submonthly disturbances propagate southwestward, the cyclonic circulation is enhanced and the anticyclonic circulation is weakened. The cyclonic circulation is associated with significant westerly wind anomalies on the equator. On days −1 and 0, the strong westerly winds are centered around 90°E on the equator, with northwesterlies near the coast of Sumatra and easterlies around 10°–15°S. The enhanced cyclonic circulation moves farther southwestward, and westerlies near the equator extend to near 70°E by day +3. In addition, strong northwesterlies continue to develop near the coast of Sumatra on days +1 to +3. These circulation anomalies in the Southern Hemisphere are also associated with weaker anomalies in the Northern Hemisphere. On days −1 and 0, a weak cyclonic circulation

TABLE 2. Correlation coefficients between mean OLR, subseasonal OLR, $\nabla \cdot (q\mathbf{U})$, SST in the southeast Indian Ocean (2.5°–12.5°S, 87.5°–102.5°E), and DMI (see text for details). The data for the period 1979–2001 are used. Linear trends are removed from the time series before the calculations.

Variables	Correlation coef
OLR (6–30 days) vs −DMI	0.86
OLR (mean) vs DMI	0.87
$\nabla \cdot (q\mathbf{U})$ vs DMI	0.85
OLR (6–30 days) vs SST (local)	0.67
OLR (mean) vs −SST (local)	0.70
$\nabla \cdot (q\mathbf{U})$ vs −SST (local)	0.66
OLR (mean) vs −OLR (6–30 days)	0.90
OLR(6–30 days) vs $-\nabla \cdot (q\mathbf{U})$	0.82
OLR (mean) vs $\nabla \cdot (q\mathbf{U})$	0.90
SST (local) vs DMI	0.90

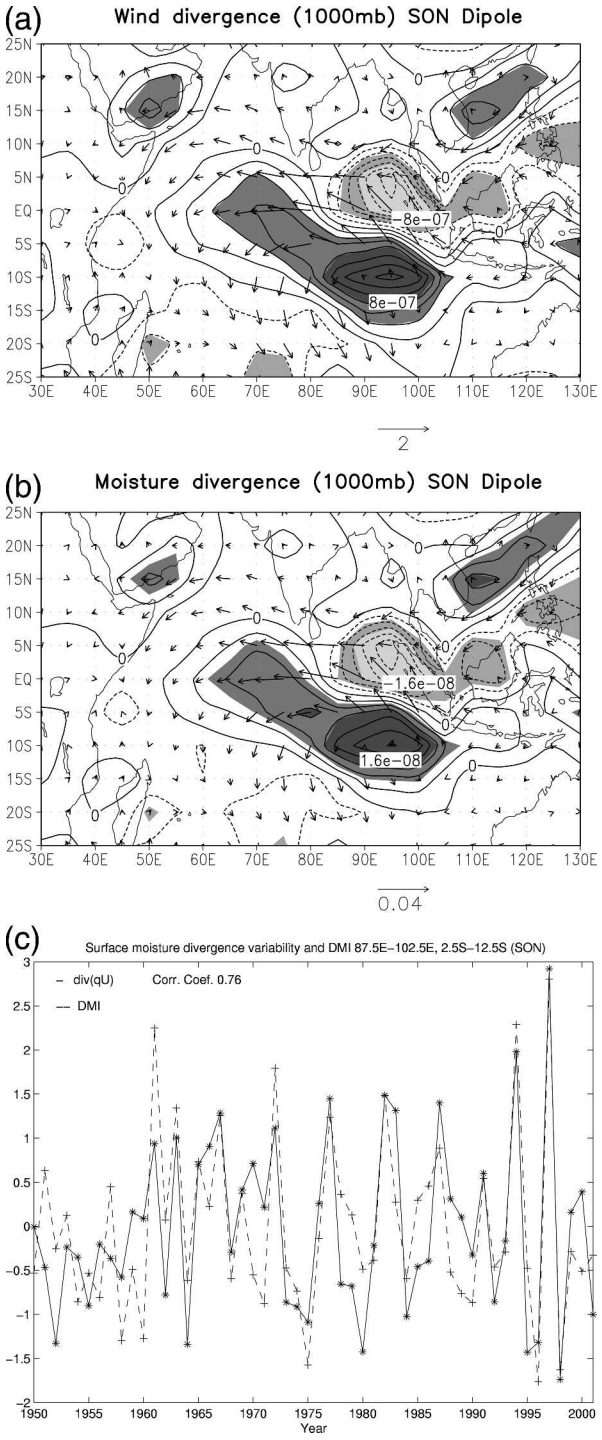

FIG. 6. (a) Winds (m s^{-1}) and wind divergence (s^{-1}) at 1000 hPa during SON regressed onto DMI. The wind divergence contour interval is 2×10^{-7} (s^{-1}). Areas where the magnitude of regressed wind divergence exceeds 4×10^{-7} (s^{-1}) are shaded. (b) Moisture flux $q\mathbf{U}$ (kg kg^{-1} m s^{-1}) and divergence $\nabla \cdot q\mathbf{U}$ (kg kg^{-1} s^{-1}) at 1000 hPa during the SON season regressed onto DMI. The moisture flux contour interval is 4×10^{-9} (kg kg^{-1} s^{-1}). Areas where the magnitude of regressed moisture divergence exceeds 5×10^{-9} are shaded. (c) Variation of $\nabla \cdot q\mathbf{U}$ for the area 2.5°–12.5°S, 87.5°–102.5°E (solid line) and DMI (dashed line) during SON. Time series of the SON mean are normalized by their standard deviations, and the means are subtracted.

centered around 5°N, 90°E is evident, which is further connected to the easterlies around 10°N in the western Pacific.

Figure 8 displays the longitude–time plot of zonal winds along 5°S from the same regression analysis as in Fig. 7. The westward propagation of submonthly disturbance with the phase speed of ~3.8 m s^{-1} is clearly seen. The zonal extent of westerly anomalies around this latitude becomes larger as the cyclonic circulation propagates westward. On day +4, regions of significant westerly anomalies cover ~30° in longitude.

The analysis suggests that during negative IOD years the active convection on the submonthly time scale in the southeast Indian Ocean is often generated, and it is associated with anomalous circulations that enhance the equatorial westerly winds in the eastern and central Indian Oceans and northwesterlies near the coast of Sumatra. To demonstrate the difference from the submonthly variability during large positive IOD events, the same regression analyses were performed using the data only in 1982, 1994, and 1997. The regressed circulation and height are shown in Fig. 9. There are almost no significant circulation or height anomalies in the southeast Indian Ocean. Also, the spatial pattern of height and circulation anomalies is dissimilar to that in Fig. 7, with positive height anomalies and a weak anticyclonic circulation around 5°S, 95°E. It should be noted that a weaker cyclonic circulation is found in the southeast Indian Ocean if all positive IOD years are included in the analysis (not shown) because there is significant submonthly convective activity in this region in some positive IOD years.

As shown in Fig. 5, both mean and submonthly convective activity are highly suppressed during these years, and thus anomalous cyclonic circulations are not present in this region. Consequently, submonthly westerly wind events are not generated on the equator. The remarkable difference in circulation anomalies between Fig. 7 and Fig. 9 explains the strong correlation of submonthly zonal wind activity with DMI near the equator. Also, the results suggest that during large IOD events the reduction of submonthly wind activity is mostly due to the reduced activity of westerly (not easterly) winds near the equator, which could have a significant impact on the upper-ocean response. Furthermore, these analyses suggest that anomalous westerlies near the equator during boreal fall in negative IOD

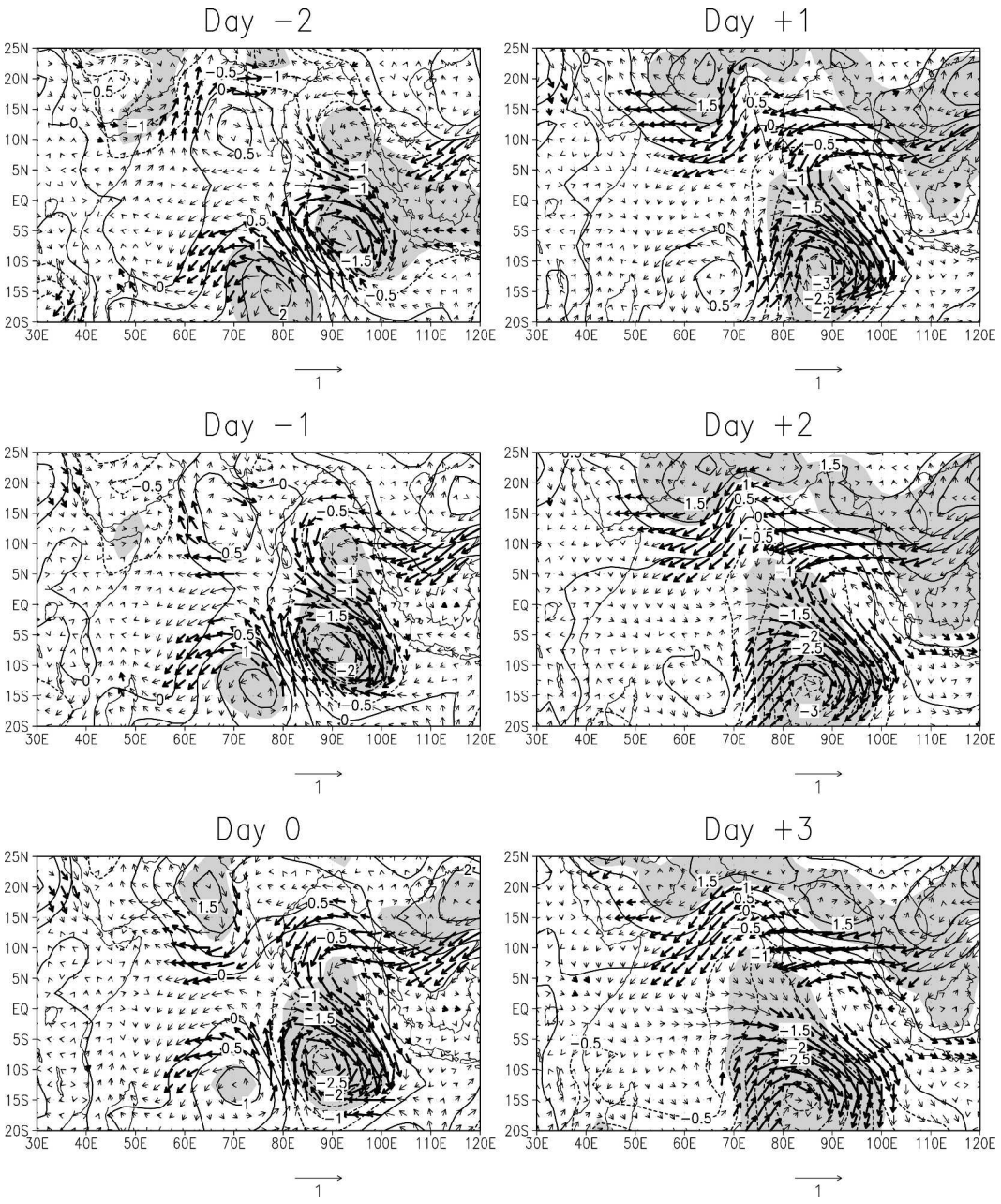

FIG. 7. 1000-hPa winds and height in the 6–30-day band during negative IOD years regressed onto submonthly (6–30 days) OLR averaged over 2.5°–12.5°S, 87.5°–102.5°E. Positive values indicate the negative correlation of winds and height with OLR in the base region. Thick arrows and shaded areas indicate that the correlation is significant at the 95% level.

years are partly caused by enhanced submonthly convective activity in the southeast Indian Ocean.

Figure 3b also shows significant positive correlations ($rr > 0.7$) between submonthly OLR variability and DMI in the southwest Indian Ocean. To examine the evolution of submonthly disturbance in this region, we have also performed the same cross-correlation analysis, in which near-surface variables are regressed onto the filtered OLR averaged over the area 2.5°–17.5°S, 42.5°–52.5°E using the data during the period of positive IOD years (not shown). The analysis shows some significant wind anomalies, including equatorial easterlies near the western boundary (~50°E), which are associated with southeasterlies around 10°S, 70°E. This suggests that the enhancement of submonthly equatorial easterlies during positive IOD years is responsible

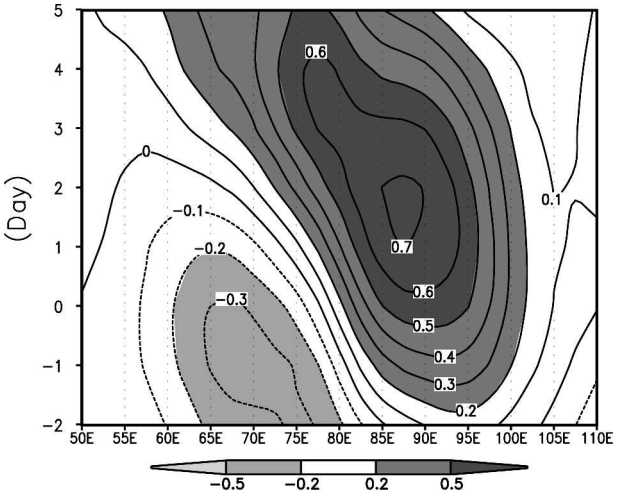

FIG. 8. A longitude–time plot of zonal wind anomalies along 5°S regressed onto submonthly OLR in the base region (2.5°–12.5°S, 87.5°–102.5°E).

for the significant correlation between submonthly zonal wind variability and DMI centered around 50°E on the equator (Fig. 3a). However, the duration of these wind anomalies is much shorter than those in the southeast Indian Ocean. Also, since convective activity in this region is much weaker than in the southeast Indian Ocean (Fig. 5), the cross-correlation analysis may not be able to extract salient features in submonthly disturbances. Hence analyses in the rest of the paper focus on submonthly disturbances in the southeast Indian Ocean where stronger variability is found both in the lower atmosphere and upper ocean (see section 5).

b. Case study: November 1996

The submonthly event during early November 1996 provides an excellent example that illustrates many features evident in the statistical analysis. Figure 10 shows 1000-hPa winds and height anomalies for the period 31 October–5 November 1996. Note that the time series are not bandpass filtered in this case. A cyclonic circulation, which is associated with westerlies on the equator, is present around 5°–10°S, 90°E on 31 October. The cyclonic circulation is then enhanced and propagates southwestward. By 4 November, regions of strong equatorial westerlies, which are associated with a negative height anomaly centered around 85°E, extend to 80°E. Also, northwesterlies are observed near the coast of Sumatra. Then these disturbances moved farther southwestward, and the negative height anomaly is centered around 10°S, 82°E on 5 November, and northwesterlies are observed on the equator. The westward propagation of this submonthly disturbance is clearly seen in the longitude–time plot of zonal winds along 5°S (Fig. 11) in which the phase speed is similar to that in the cross-correlation analysis.

As described above, many of the features identified by the statistical analysis are evident in the submonthly event during early November 1996. While timing and spatial structure varies somewhat from event to event, similar events are often seen in other years (not shown), suggesting that the regression analysis is able to effectively isolate salient features in the submonthly events in this region. During this submonthly event (November 1996), significant circulation and height anomalies are also found in the Northern Hemisphere (around 15°N, 110°E), but these disturbances are not symmetric with regard to the equator. Hence this submonthly event may not be described as convectively coupled equatorial Rossby waves (e.g., Wheeler and Kiladis 1999). However, it should be noted that some of the submonthly events in this region are associated with a twin cyclone (not shown), in which the spatial structure is similar to equatorial Rossby waves. Further analyses are necessary to examine the generation mechanism and dynamics of these submonthly disturbances in this region.

It should also be noted that this submonthly event (November 1996) in the southeast Indian Ocean is not associated with the MJO. However, some of the similar submonthly wind events co-occurred with the MJO. For instance, similar submonthly wind anomalies associated with a cyclonic circulation in the southeast Indian Ocean are observed in early December 1996 (not shown). At the same time, strong intraseasonal convection associated with the MJO is generated in the central and eastern Indian Ocean. The maximum equatorial westerly associated with the submonthly event occurs at the nearly same time and location (~75°E) as the westerly associated with the MJO. This suggests that westward-moving submonthly disturbances identified by statistical analysis could sometimes interact with and influence the MJO, which then propagates eastward and may affect the Pacific Ocean (see Roundy and Frank 2004). Further analyses are currently being conducted to pursue this problem.

5. Ocean response

It is demonstrated in the previous section that cyclonic circulations often developed in the southeast Indian Ocean during negative IOD years, which are associated with westerly winds on the equator and northwesterlies near the coast of Sumatra. In this section, upper-ocean response to submonthly wind events is discussed using the OGCM experiments.

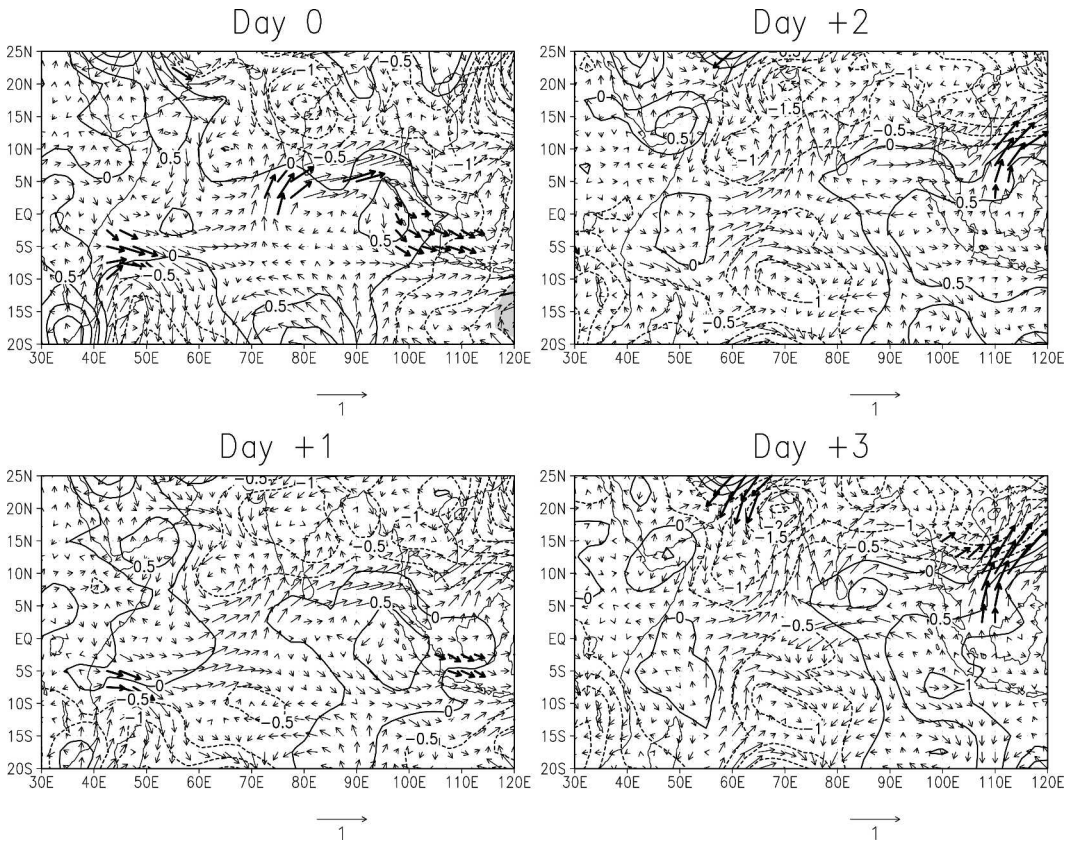

FIG. 9. Same as in Fig. 7, except that only the data during 1982, 1994, and 1997 are used.

The OGCM used in this study is the Hybrid Coordinate Ocean Model (HYCOM; e.g., Bleck 2002). The hybrid coordinate is the one that is isopycnal in the open, stratified ocean but that smoothly reverts to a terrain-following coordinate in the shallow coastal regions and z-level coordinates in the mixed layer and/or unstratified seas. The model includes the K profile parameterization (KPP) of the upper-ocean boundary layer (Large et al. 1994). Further details of model physics and numerical schemes are found in Bleck (2002).

The tropical Indian Ocean basin HYCOM (north of 30°S) was integrated with 3-day mean surface forcing fields for the period 1988–2000. The wind stress is calculated using surface winds from the NCEP–NCAR reanalysis. The model's ability to simulate subseasonal upper-ocean currents and sea surface height (SSH) is demonstrated by Han et al. (2004) and Han (2005). In this study, the output from the model experiment during the period 1991–99 is analyzed. Further details of model configuration and experiments are found in Han et al. (2004).

Figure 12a shows the average standard deviation of bandpass-filtered (6–30 days) surface zonal currents during the SON season. Strong submonthly variability is mostly found in the eastern part of the basin between 5°N and 5°S besides regions of western boundary currents. The intensity of submonthly zonal currents in the eastern Indian Ocean is well correlated with the activity of submonthly winds (Fig. 12b). In particular, the activity of submonthly surface zonal currents is largely reduced during the 1997 IOD event when submonthly zonal wind activity is weakest.

To examine upper-ocean variability associated with atmospheric submonthly disturbances, the same cross-correlation analysis described in section 4 was performed. The time series of surface zonal and meridional velocities and SSH anomalies are first bandpass filtered on the submonthly time scale (6–30 days). Six years of the filtered time series during the SON season in negative IOD years (DMI < 0) are then regressed onto the filtered (6–30 days) OLR in the base region 2.5°–12.5°S, 87.5°–102.5°E (Fig. 13).

On day -1, southeastward currents around 2°–4°S and eastward currents around 5°–6°S between 90° and 100°E begin to develop. Southward currents are also found in the Northern Hemisphere around 3°N, 90°E.

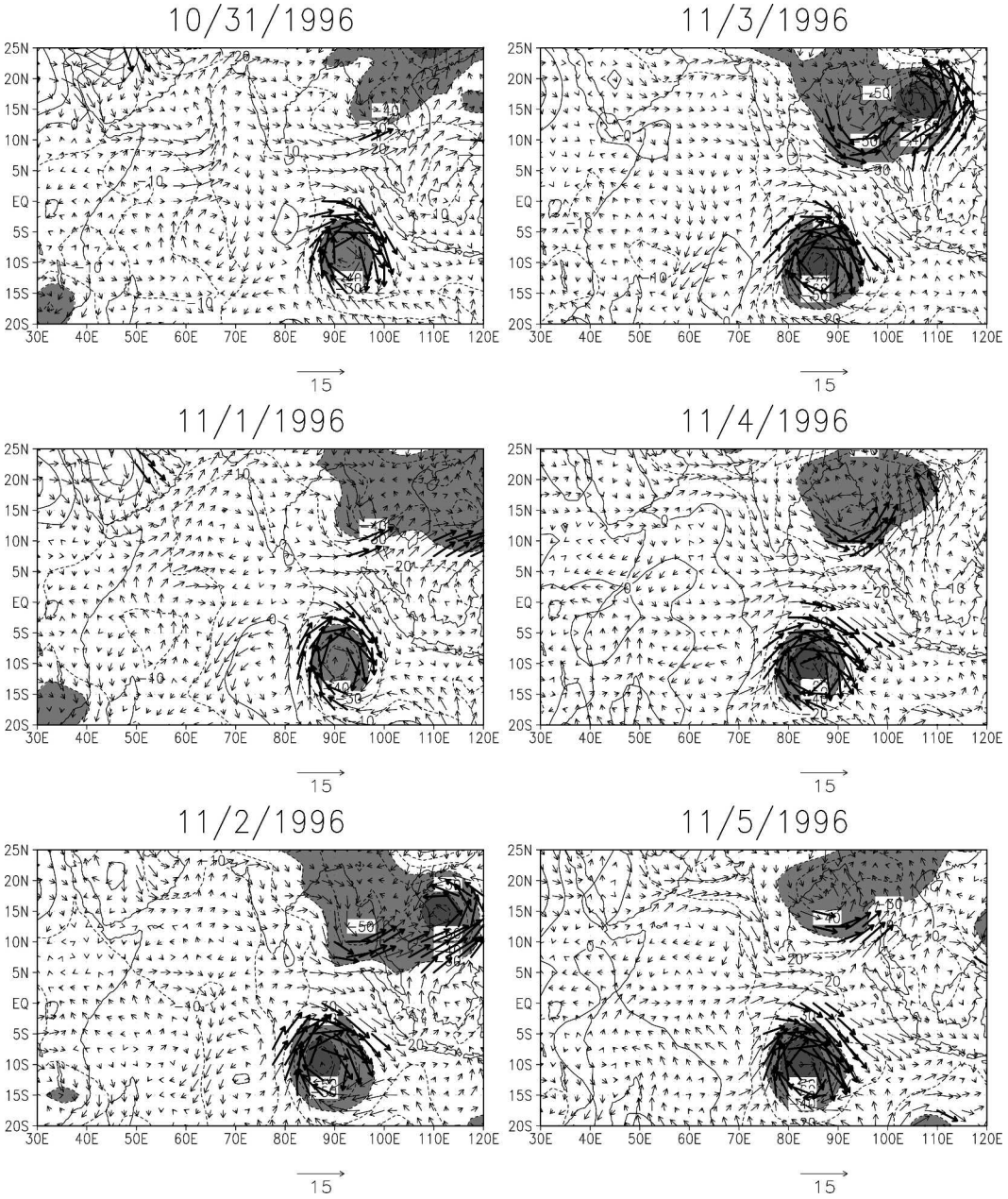

FIG. 10. Wind (m s^{-1}) and height anomalies (m) during 31 Oct–5 Nov 1996. Thick arrows indicate wind speed anomalies greater than 7 m s^{-1}. The dark and light shadings indicate the magnitude of height anomalies greater than 60 and 30 m, respectively.

As the atmospheric cyclonic circulation is enhanced (Fig. 7), strong eastward currents around 2°–5°S between 90° and 100°E are generated, in association with strong northwesterlies in this region. These eastward currents are connected to southeastward currents on the equator around 90°E and southwestward currents around 5°N (day 0 to day +3). In contrast to the eastward currents east of 90°E during this period, weaker northwestward and westward currents are generated west of 85°E between the equator and 10°S (day 0 to +2) where southerly and southwesterly anomalies are observed (Fig. 7). As the cyclonic circulation propagates westward, regions of eastward current extend farther west. By day +4, eastward currents are generated in most of the areas east of 70°E between the equator and 10°S.

Significant SSH anomalies associated with these current anomalies are also found. During days 0 to +2, large positive SSH anomalies develop around 2°–4°S,

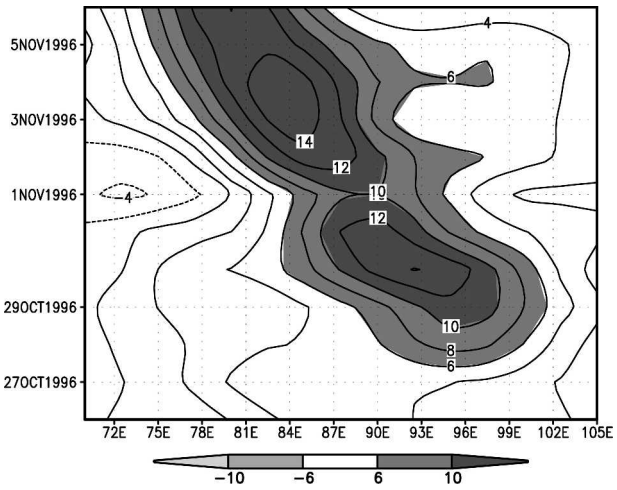

FIG. 11. A longitude–time plot of zonal wind anomalies (m s^{-1}) along 5°S during 26 Oct–6 Nov 1996.

90°–95°E, with strong convergence of surface current anomalies. As eastward currents around 2°–5°S become strong, positive SSH anomalies also develop along the coast of Sumatra between 4°N and 6°S (day +2 to day +4). During this period, large negative SSH anomalies associated with strong divergence of surface currents are also found around 8°S, 90°–95°E and 4°N, 90°E.

These analyses suggest that significant upper-ocean current and SSH anomalies can be generated by a typical atmospheric submonthly disturbance in the southeast Indian Ocean. Major features of upper-ocean variability described above are also identified during early November 1996 when strong atmospheric submonthly disturbances are observed in this region. Figure 14 shows surface current and SSH anomalies on 29 October, 1 November, and 4 November relative to those on 26 October when wind anomalies begin to develop in the southeast Indian Ocean (Fig. 11). Note that the time series are not bandpass filtered in this case. Anomalous eastward currents around 5°S, 95°–100°E and southward currents between the equator and 5°N around 90°–95°E begin to develop on 29 October. Then strong eastward currents are generated around 3°–8°S, 90°E on 1 November. These current anomalies continue to develop, and the eastward currents that exceed 40 cm s^{-1} are found around 3°–8°S, 90°E on 4 November and are associated with strong northwesterlies in this region (Fig. 10). These eastward currents are connected to southward currents on the equator around 85°–90°E and southwestward currents around 2°N. Northward and northwestward currents are found west of 80°E between 4° and 8°S where southwesterly anomalies are observed during 1–4 November (Fig. 10).

In association with these surface current anomalies, significant SSH anomalies are also generated during this period. Large negative SSH anomalies centered around 8°S, 90°E begin to develop on 1 November, with strong divergence of surface currents. At the same time, positive SSH anomalies appear near the coast of Sumatra between 2°N and 8°S. These positive and negative SSH anomalies further develop as the surface current divergence and convergence are enhanced by 4 November. SSH anomalies near the coast may be caused by a combination of local downwelling generated by northwesterly wind anomalies near the coast (Fig. 10) and coastal Kelvin waves propagated from the equator. As described above, major features in statistically derived relationships are evident during the period of this submonthly event, suggesting that the spatial pattern and evolution of the upper ocean in response to a typical atmospheric submonthly disturbance in this region can be effectively isolated by the cross-correlation analysis.

Aside from strong eastward currents around 3°–8°S where strong winds associated with the cyclonic circulation are observed, strong southeastward currents on the equator around 91°E, which exceed 60 cm s^{-1}, are also generated during this event (Fig. 14c). The strength of the currents on the equator is equivalent to zonal current anomalies around 3°–8°S, although the zonal winds are weaker on the equator during this event. Since strong zonal jets can directly be driven by zonal winds within the equatorial Rossby radius (~2°; Yoshida 1959), the dynamical ocean response is sensitive to the meridional extent of zonal winds associated with the cyclonic circulation. Hence even a small event-to-event variation in latitudinal scale and location of subseasonal disturbance in this area can cause significant differences in the upper-ocean response.

Upper-ocean circulation and thermocline depth anomalies in response to submonthly winds could cause SST anomalies through vertical and horizontal advection of heat and entrainment. We have also performed the same regression analysis using SSTs from the model output to examine the evolution of SST anomaly associated with submonthly disturbances (not shown). While some indication of warming near the coast of Sumatra is evident, the signal is not as clear as in the current and SSH anomalies. This suggests that at least the ocean response to atmospheric submonthly winds in the southeast Indian Ocean is not a primary cause of IOD events. However, it is possible that pronounced submonthly SSH and current anomalies on the submonthly time scale could feed back on some of the IOD events. During the submonthly event in November 1996, the positive SSH anomalies extend south of the equator along the coast of Sumatra (Fig. 14c) where

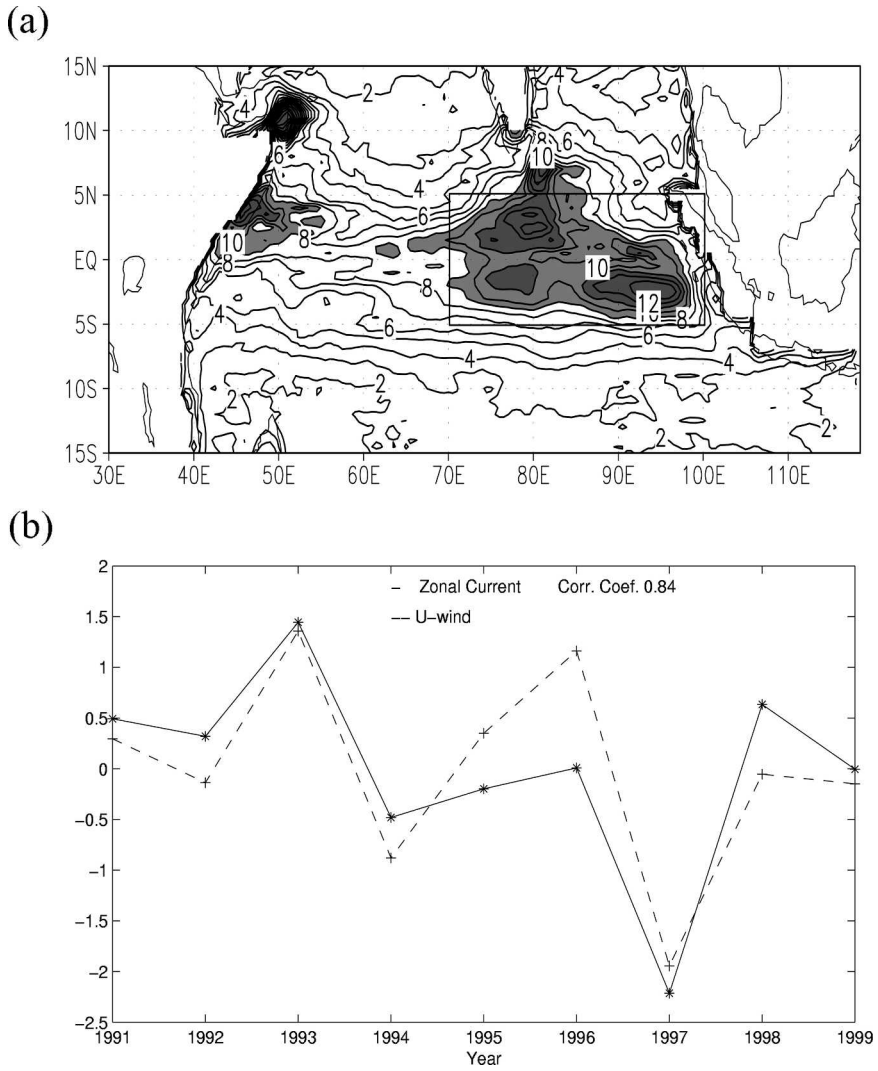

FIG. 12. (a) Standard deviation of surface zonal current (cm s^{-1}) in the 6–30-day band during SON for the period 1991–99. (b) Variations of the intensity of submonthly surface zonal current (solid line) and 1000-hPa zonal wind (dashed line) variability for the area 5°N–5°S, 70°–100°E. The intensity of submonthly variability is measured by standard deviation of bandpass-filtered (6–30-day) time series. Time series of the SON mean are normalized by their standard deviations, and the means are subtracted.

large SST anomalies are generally observed in association with IOD events. The positive SSH anomalies (and thus deep thermocline) on the submonthly time scale could enhance the warming during negative dipole years in this region. Since submonthly wind activity is highly correlated with the IOD, they could provide the positive feedback onto the SST dipole variability. SST changes due to subseasonal variability of thermocline depth and heat advection may strongly depend on upper-ocean basic states such as the depth of main thermocline and horizontal temperature gradient, which vary from event to event. Further model experiments and diagnoses are required to investigate the overall impact of subseasonal wind variability on the IOD, which is one of our ongoing studies.

6. Conclusions and discussion

Interannual variation of the intensity of atmospheric subseasonal (6–90-day) variability over the tropical Indian Ocean and its relation with SST dipole variability are examined using winds, geopotential height, and humidity from the NCEP–NCAR reanalysis, OLR, and the monthly SST analysis. During the boreal fall season, activity of subseasonal winds in the equatorial Indian Ocean is well correlated with the SST dipole variability.

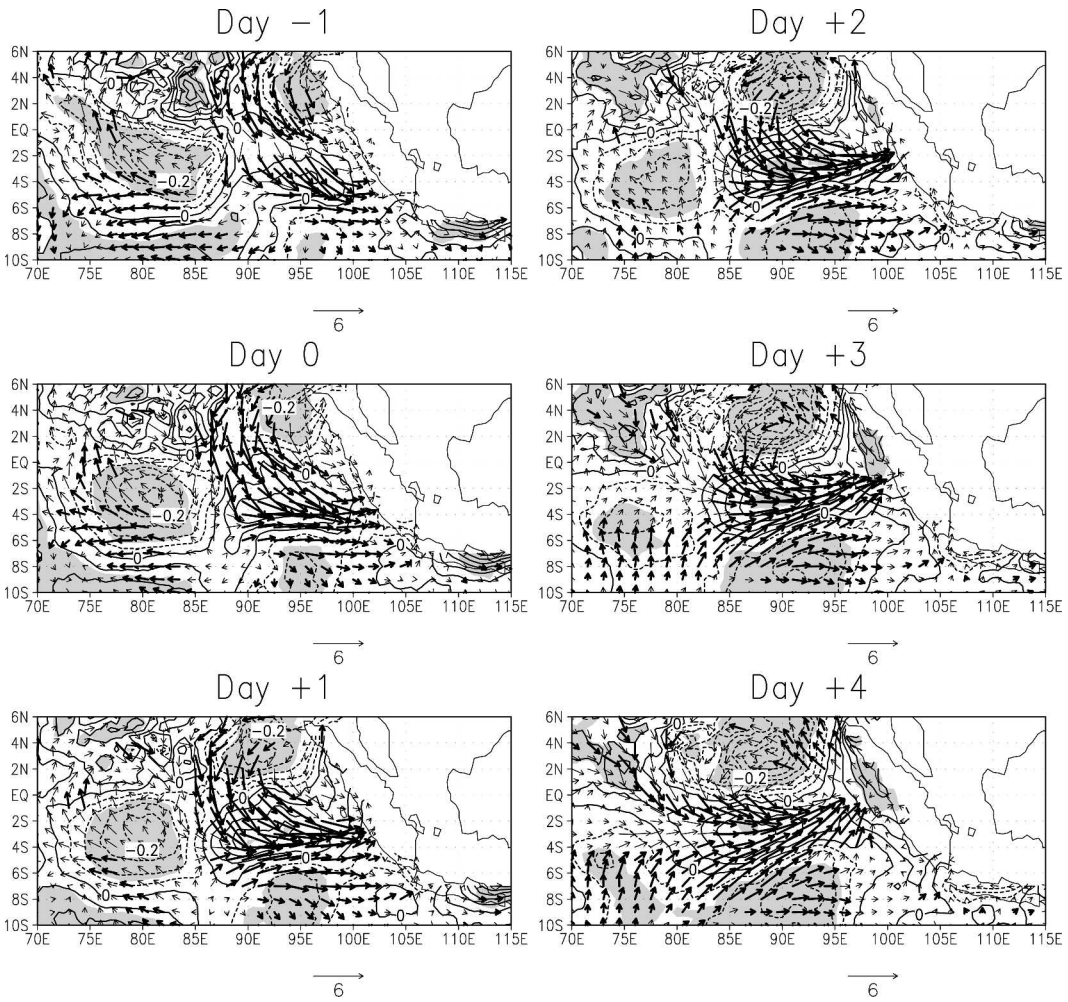

FIG. 13. Surface currents (cm s^{-1}), and SSH anomalies (cm) in the 6–30-day band during negative IOD years regressed onto submonthly (6–30 days) OLR averaged over 2.5°–12.5°S, 87.5°–102.5°E for days −1 to +4. Positive values indicate the negative correlation of surface currents and SSH with OLR in the base region. Thick arrows and shaded areas indicate that the correlation is significant at the 90% level.

The wind variability on the submonthly (6–30 days) time scale is mostly responsible for the strong correlation. During positive dipole events when warm SST anomalies in the west and cold anomalies in the east are found (Fig. 1a), submonthly wind activity near the equator and convective activity in the southeast Indian Ocean are largely reduced. While mean and submonthly convective activity in this region are well correlated with the local SST, the correlations with DMI are significantly higher. This suggests that basin-scale SST gradients and wind anomalies play an important role in controlling interannual variations of convective activity in the southeast Indian Ocean where the anomalous convergence of surface moisture associated with dipole events is at its maximum.

To describe the spatial structure and time evolution of submonthly disturbances and their relation to the SST dipole, wind and height anomalies are regressed onto the time series of submonthly OLR in the southeast Indian Ocean. During negative dipole years, submonthly convection generated in the southeast Indian Ocean is associated with a cyclonic circulation. These submonthly disturbances propagate southwestward, which generate equatorial westerly winds in the eastern and central Indian Ocean and northwesterlies near the coast of Sumatra. During large positive dipole years, submonthly convective activity is largely suppressed in the southeast Indian Ocean and thus no equatorial westerly is generated. Many features of submonthly disturbances identified by the statistical analysis are evident in individual events including the event observed in early November 1996.

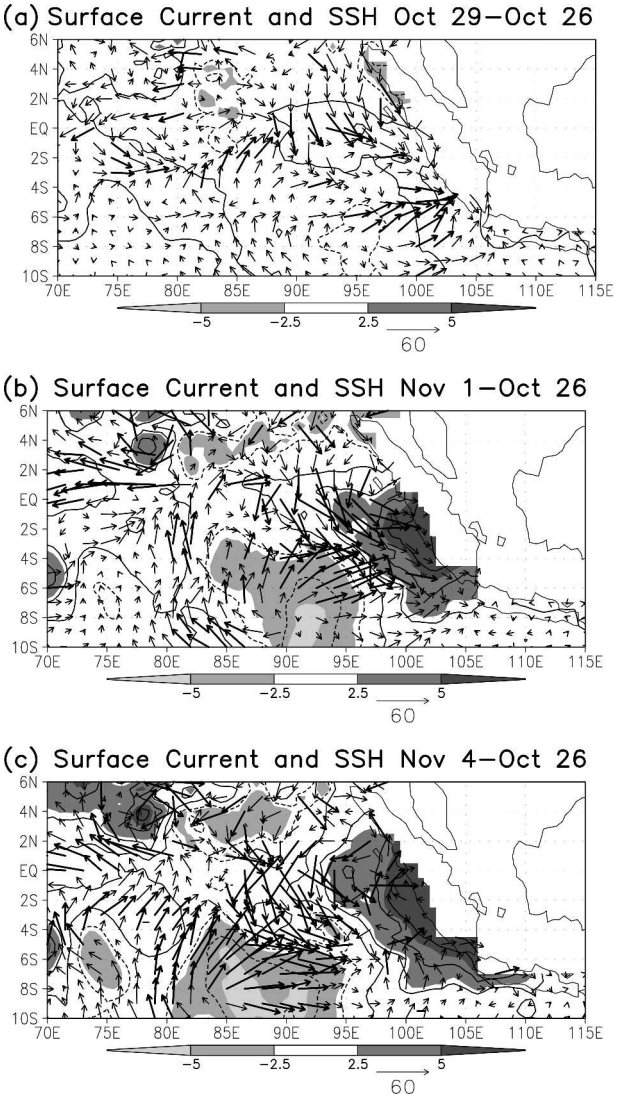

FIG. 14. Surface current (cm s^{-1}), and SSH anomalies (cm) on (a) 29 Oct, (b) 1 Nov, and (c) 4 Nov 1996 relative to those on 26 Oct 1996. Thick arrows indicate currents stronger than 25 cm s^{-1}.

The ocean response to atmospheric submonthly disturbances is examined using the OGCM experiments forced with observed winds. Submonthly winds can directly generate large surface current anomalies, including strong eastward currents centered around 3°–4°S in the southeast Indian Ocean. Strong zonal currents on the equator are also generated during the submonthly event in November 1996. Westerlies on the equator and northwesterlies near the coast also can cause the increase of SSH (and thus downwelling) along the coast of Sumatra where SST anomalies associated with dipole events are at a maximum. Consequently, these positive SSH anomalies could possibly enhance the warming in these regions, and thus they may provide positive feedback onto dipole variability.

Aside from dynamical response of the upper ocean, subseasonal winds can enhance surface evaporative cooling because wind speed is increased because of the high-frequency variability (Kessler and Kleeman 2000; Shinoda and Hendon 2002). Stronger subseasonal winds during negative dipole years could significantly enhance evaporative cooling in the southeast Indian Ocean, and thus they could provide a negative feedback on the SST dipole. The relative importance of surface heat flux and dynamical response produced by subseasonal disturbance in this region is unknown, and it may vary from event to event. To fully examine the overall impact of atmospheric subseasonal variability on the Indian Ocean dipole requires further model experiments and diagnoses, which is a part of our ongoing and future research.

While the Indian Ocean dipole variability is well correlated with ENSO (e.g., Baquero-Bernal et al. 2002; see also Table 1), the relationship between the strength of ENSO and the strength of SST dipole is not linear (e.g., Shinoda et al. 2004b). In other words, some large ENSO events are associated with modest SST dipoles and some modest ENSO events are associated with strong SST dipoles. This suggests that air–sea coupled processes inherent to the Indian Ocean play an important role in determining the amplitude of dipole events. The feedback between atmospheric subseasonal variability and interannual SST discussed in this study could be one possible mechanism that influences the evolution and amplitude of dipole variability. For instance, SST anomalies in the eastern Indian Ocean could be initially generated by modest ENSO events through an atmospheric bridge mechanism (Shinoda et al. 2004a), and the large SST anomalies could be developed through positive feedback between subseasonal and interannual variability. Coupled modeling studies are necessary to further investigate these feedback processes.

Acknowledgments. Valuable discussions with George Kiladis and Jialin Lin are greatly appreciated. Constructive comments by two reviewers helped improve the original draft of this paper. Toshiaki Shinoda is supported by CLIVAR-Pacific grants from NOAA's Office of Global Programs and NSF OCE-0453046, and Weiqing Han is supported by NSF OCE-0136836.

REFERENCES

Baquero-Bernal, A., M. Latif, and S. Legutke, 2002: On dipolelike variability of sea surface temperature in the tropical Indian Ocean. *J. Climate,* **15,** 1358–1368.

Bergman, J. W., H. H. Hendon, and K. M. Weickmann, 2001: Intraseasonal air–sea interactions at the onset of El Niño. *J. Climate,* **14,** 1702–1719.

Bleck, R., 2002: An oceanic general circulation model framed in Hybrid Isopycnic-Cartesian Coordinates. *Ocean Modell.,* **4,** 55–88.

Chatterjee, P., and B. N. Goswami, 2004: Structure, genesis and scale selection of the tropical quasi-biweekly mode. *Quart. J. Roy. Meteor. Soc.,* **130,** 1171–1194.

Dickinson, M., and J. Molinari, 2002: Mixed Rossby-gravity waves and western Pacific tropical cyclogenesis. Part I: Synoptic evolution. *J. Atmos. Sci.,* **59,** 2183–2196.

Duchon, C. E., 1979: Lanczos filtering in one and two dimensions. *J. Appl. Meteor.,* **18,** 1016–1022.

Fink, A., and P. Speth, 1997: Some potential forcing mechanisms of the year-to-year variability of the tropical convection and its intraseasonal (25–70-day) variability. *Int. J. Climatol.,* **17,** 1513–1534.

Gruber, A., and A. F. Krueger, 1984: The status of the NOAA outgoing longwave radiation data set. *Bull. Amer. Meteor. Soc.,* **65,** 958–962.

Han, W., 2005: Origins and dynamics of the 90-day and 30–60-day variations in the equatorial Indian Ocean. *J. Phys. Oceanogr.,* **35,** 708–728.

——, D. M. Lawrence, and P. J. Webster, 2001: Dynamical response of equatorial Indian Ocean to intraseasonal winds: Zonal flow. *Geophys. Res. Lett.,* **28,** 4215–4218.

——, P. Webster, R. Lukas, P. Hacker, and A. Hu, 2004: Impact of atmospheric intraseasonal variability in the Indian Ocean: Low-frequency rectification in equatorial surface current and transport. *J. Phys. Oceanogr.,* **34,** 1350–1372.

Hartmann, D. L., M. L. Michelsen, and S. A. Klein, 1992: Seasonal variations of tropical intraseasonal oscillations: A 20–25-day oscillation in the western Pacific. *J. Atmos. Sci.,* **49,** 1277–1289.

Hendon, H. H., and B. Leibmann, 1994: Organization of convection within Madden-Julian oscillation. *J. Geophys. Res.,* **99,** 8073–8083.

——, C. Zhang, and J. Glick, 1999: Interannual variation of the Madden–Julian oscillation during austral summer. *J. Climate,* **12,** 2538–2550.

Kalnay, E., and Coauthors, 1996: The NCEP/NCAR 40-Year Reanalysis Project. *Bull. Amer. Meteor. Soc.,* **77,** 437–471.

Kessler, W. S., and R. Kleeman, 2000: Rectification of the Madden–Julian oscillation into the ENSO cycle. *J. Climate,* **13,** 3560–3575.

Kiladis, G. N., and K. M. Weickmann, 1992: Circulation anomalies associated with tropical convection during northern winter. *Mon. Wea. Rev.,* **120,** 1900–1923.

——, and M. Wheeler, 1995: Horizontal and vertical structure of observed tropospheric equatorial Rossby waves. *J. Geophys. Res.,* **100,** 22 981–22 997.

——, G. A. Meehl, and K. M. Weickmann, 1994: Large-scale circulation associated with westerly wind bursts and deep convection over the western equatorial Pacific. *J. Geophys. Res.,* **99,** 18 527–18 554.

Large, W. G., J. C. McWilliams, and S. C. Doney, 1994: Oceanic vertical mixing: Review and a model with a nonlocal boundary layer parameterization. *Rev. Geophys.,* **32,** 363–403.

Lau, K. M., and P. H. Chan, 1988: Intraseasonal and interannual variations of tropical convection: A possible link between the 40–50 day oscillation and ENSO? *J. Atmos. Sci.,* **45,** 506–521.

Liebmann, B., and H. H. Hendon, 1990: Synoptic-scale disturbances near the equator. *J. Atmos. Sci.,* **47,** 1463–1479.

Lyons, S. W., 1981: Planetary-scale aspects of outgoing longwave radiation and vorticity over the global tropics during winter. *Mon. Wea. Rev.,* **109,** 1773–1787.

Madden, R. A., and P. R. Julian, 1972: Description of global-scale circulation cells in the tropics with a 40–50 day period. *J. Atmos. Sci.,* **29,** 1109–1123.

Mathews, A. J., and G. N. Kiladis, 1999: The tropical–extratropical interaction between high-frequency transients and the Madden–Julian oscillation. *Mon. Wea. Rev.,* **127,** 661–677.

Matsuno, T., 1966: Quasi-geostrophic motions in the equatorial area. *J. Meteor. Soc. Japan,* **44,** 25–43.

Murakami, T., 1972: Equatorial tropospheric waves induced by diabatic heat sources. *J. Atmos. Sci.,* **29,** 827–836.

——, 1980: Temporal variations of satellite-observed outgoing longwave radiation over the winter monsoon region. Part I: Long-period (15–30 day) oscillations. *Mon. Wea. Rev.,* **108,** 408–426.

——, and M. Frydrych, 1974: On the preferred period of upper wind fluctuations during the summer monsoon. *J. Atmos. Sci.,* **31,** 1549–1555.

Numaguti, A., 1995: Characteristics of 4-to-20-day-period disturbances observed in the equatorial Pacific during the TOGA COARE IOP. *J. Meteor. Soc. Japan,* **73,** 353–377.

Oort, A. H., and J. J. Yienger, 1996: Observed interannual variability in the Hadley circulation and its connection to ENSO. *J. Climate,* **9,** 2751–2767.

Reed, R. J., and E. E. Recker, 1971: Structure and properties of synoptic-scale wave disturbances in the equatorial western Pacific. *J. Atmos. Sci.,* **28,** 1117–1133.

Roundy, P. E., and W. M. Frank, 2004: Effects of low-frequency wave interactions on intraseasonal oscillations. *J. Atmos. Sci.,* **61,** 3025–3040.

Saji, N. H., B. N. Goswami, P. N. Vinayachandran, and T. Yamagata, 1999: A dipole mode in the tropical Indian Ocean. *Nature,* **401,** 360–363.

Schiller, A., and J. S. Godfrey, 2003: Indian Ocean intraseasonal variability in an ocean general circulation model. *J. Climate,* **16,** 21–39.

Shinoda, T., and H. H. Hendon, 1998: Mixed layer modeling of intraseasonal variability in the tropical western Pacific and Indian Oceans. *J. Climate,* **11,** 2668–2685.

——, and ——, 2001: Upper-ocean heat budget in response to the Madden–Julian oscillation in the western equatorial Pacific. *J. Climate,* **14,** 4147–4165.

——, and ——, 2002: Rectified wind forcing and latent heat flux produced by the Madden-Julian oscillation. *J. Climate,* **15,** 3500–3508.

——, ——, and J. Glick, 1998: Intraseasonal variability of surface fluxes and sea surface temperature in the tropical western Pacific and Indian Ocean. *J. Climate,* **11,** 1685–1702.

——, ——, and ——, 1999: Intraseasonal surface fluxes in the tropical western Pacific and Indian Ocean from NCEP reanalyses. *Mon. Wea. Rev.,* **127,** 678–693.

——, M. A. Alexander, and H. H. Hendon, 2004a: Remote response of the Indian Ocean to interannual SST variations in the tropical Pacific. *J. Climate,* **17,** 362–372.

——, H. H. Hendon, and M. A. Alexander, 2004b: Surface and subsurface dipole variability in the Indian Ocean and its relation with ENSO. *Deep-Sea Res.,* **51,** 619–635.

Smith, T. M., and R. W. Reynolds, 2004: Improved extended reconstruction of SST (1854–1997). *J. Climate,* **17,** 2466–2477.

Straub, K., and G. N. Kiladis, 2003: Interactions between the bo-

real summer intraseasonal oscillation and higher-frequency tropical wave activity. *Mon. Wea. Rev.,* **131,** 945–960.

Takayabu, Y. N., and T. Nitta, 1993: 3–5 day-period disturbances coupled with convection over the tropical Pacific Ocean. *J. Meteor. Soc. Japan,* **71,** 221–246.

Waliser, D. E., R. Murtugudde, and L. Lucas, 2003: Indo-Pacific Ocean response to atmospheric intraseasonal variability. Part I: Austral summer and the Madden-Julian Oscillation. *J. Geophys. Res.,* **108,** 3160, doi:10.1029/2002JC001620.

Webster, P. J., and R. Lukas, 1992: TOGA COARE: The Coupled Ocean–Atmosphere Response Experiment. *Bull. Amer. Meteor. Soc.,* **73,** 1377–1416.

——, A. M. Moore, J. P. Loschnig, and R. R. Leben, 1999: Coupled ocean-atmosphere dynamics in the Indian Ocean during 1997–98. *Nature,* **401,** 356–360.

Wheeler, M., and G. N. Kiladis, 1999: Convectively coupled equatorial waves: Analysis of clouds and temperature in the wavenumber–frequency domain. *J. Atmos. Sci.,* **56,** 374–399.

——, ——, and P. J. Webster, 2000: Large-scale dynamical fields associated with convectively coupled equatorial waves. *J. Atmos. Sci.,* **57,** 613–640.

Wyrtki, K., 1973: An equatorial jet in the Inidan Ocean. *Science,* **181,** 262–264.

Yoshida, K., 1959: A theory of the Cromwell current and of the equatorial upwelling—An interpretation in a similarity to a coastal circulation. *J. Oceanogr. Soc. Japan,* **15,** 159–170.

Yu, L., R. A. Weller, and W. T. Liu, 2003: Case analysis of a role of ENSO in regulating the generation of westerly wind bursts in the western equatorial Pacific. *J. Geophys. Res.,* **108,** 3128, doi:10.1029/2002JC001498.